Journal of Electroanalytical Chemistry 783 (2016) 258–267

Contents lists available at ScienceDirect

Journal of Electroanalytical Chemistry

journal homepage: www.elsevier.com/locate/jelechem

Characterization of the surface redox process of caffeic acid adsorbed at glassy carbon electrodes modified with partially reduced graphene oxide

Sebastián Noel Robledo [a], Jimena Claudia López [b], Adrian Marcelo Granero [b], Maximiliano Andrés Zensich [b], Gustavo Marcelo Morales [b], Héctor Fernández [b,*], María Alicia Zon [b,*]

[a] Departamento de Tecnología Química, Facultad de Ingeniería, Universidad Nacional de Río Cuarto, Agencia Postal N 3 (5800)—Río Cuarto, Argentina.
[b] Departamento de Química, Facultad de Ciencias Exactas, Físico-Químicas y Naturales, Universidad Nacional de Río Cuarto, Agencia Postal N 3 (5800)—Río Cuarto, Argentina.

ARTICLE INFO

Article history:
Received 10 August 2016
Received in revised form 1 November 2016
Accepted 7 November 2016
Available online 14 November 2016

Keywords:
Caffeic acid
Partially reduced graphene oxide
Cyclic voltammetry
Square wave voltammetry
Thermodynamic and kinetics parameters

ABSTRACT

This paper describes for the first time the caffeic acid (CA) electrochemical oxidation in 1.0 M $HClO_4$ and phosphate buffer solutions (PBS) of different pH at glassy carbon electrodes (GCE) modified with electrochemically partially reduced graphene oxide (GCE/ePRGO) using cyclic and square wave voltammetries. A quasi-reversible surface redox couple was found in all reaction media at this modified electrode. The Box-Behnken design (BBD) statistical experiments and the surface methodology (RSM) were used to optimize experimental variables to generate the GCE/ePRGO. Atomic force microscopy (AFM) and electrochemical impedance spectroscopy (EIS) were used as the techniques to characterize the surface of modified electrodes. EIS was also used to determine a tentative electrochemical area for the GCE/ePRGO.
The Frumkin adsorption isotherm was the best which describes the specific interaction of CA with CGE/ePRGO. The thermodynamic and kinetics of the surface redox couple were studied in 1.0 M $HClO_4$. Therefore, we used the methods of the "quasi-reversible maximum" and the "splitting of the net SW voltammetric peak" to obtain information about the thermodynamic and kinetics of this surface redox couple. Averages values obtained for the formal potential and the anodic transfer coefficient were (0.638 ± 0.005) V and (0.58 ± 0.06), respectively. A value of 40 s^{-1} was obtained for the overall formal rate constant. For comparison, CA electrochemical responses were also studied at bare GCE, and GCE modified with a dispersion of graphene oxide (GCE/GO).
© 2016 Elsevier B.V. All rights reserved.

1. Introduction

Caffeic acid or 3-(3.4-dihydroxyphenyl)-2-propenoic acid (CA) is a phenolic acid (Fig. 1), which is found in various agricultural products such as coffee [1], teas [2], potatoes, grains, vegetables, fruits and orange juices [3]. CA is also often found in herbs [4] or wines [5].

Thus, CA is a biomolecule derived from plants. It has a variety of interesting properties, including *anti*-inflammatory, anticancer, anti-depressive, antiviral, antioxidant, anti-pruritic, and anti-tumor effects [6–11].

Moreover, it is usual to determine the antioxidant activity of a given matrix based on the total polyphenolic content (TPC), without the individual contribution of the different components. The CA is often chosen as a reference compound to evaluate the TPC [12]. Thus, it is of great interest to study the CA electrochemical behavior at different electrode surfaces. Giacomelli et al. [13]. studied the CA electro-oxidation in aqueous solutions in the pH range from 2.0 to 8.5 at bare glassy carbon electrodes (GCE) to propose an electro-oxidation mechanism in aqueous solutions and to characterize the probable products. These authors found that the electrode process is diffusion controlled, and that two electrons are involved in the CA electro-oxidation mechanism at all pH's studied. They proposed that the corresponding o-quinone should be the main product formed. However, they also found that the stability of the o-quinone electrochemically generated depends on the pH, being greater at pH ≤ 5.5. Therefore, these authors proposed that the CA electro-oxidation mechanism is $2e^-$, $2H^+$ at pH lower than about 5.5. Moreover, a variety of methods has also been developed to determine CA in real samples [14–17]. In this sense, the modification of electrode surfaces with nano-materials has been studied in order to increase their conductivity properties, and their electro-catalytic activities [14,15,18].

The use of graphene in several areas of science has grown in recent years. The great interest in this material is based on its outstanding physical properties such as quantum electronic transport, high mobility, and high elasticity [19]. Graphene derivatives are also very important for the development of various investigations [20–24]. Graphene oxide (GO) is an oxidized form of graphene, which contains polar organic groups such as epoxide, carbonyl, carboxyl, and hydroxyl among

* Corresponding authors.
E-mail addresses: hfernandez@exa.unrc.edu.ar, hfernandezster@gmail.com (H. Fernández), azon@exa.unrc.edu.ar, alicia_zon@hotmail.com (M.A. Zon).

http://dx.doi.org/10.1016/j.jelechem.2016.11.012
1572-6657/© 2016 Elsevier B.V. All rights reserved.

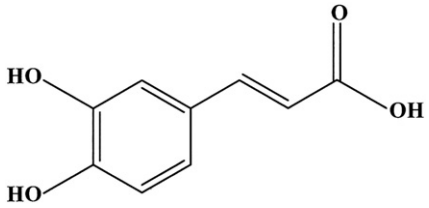

Fig. 1. Chemical structure of caffeic acid.

other, allowing its reduction by different routes. These polar organic groups have high hydrophilicity, making that the GO can be easily dispersed in aqueous suspensions [25]. When the GO is reduced through an appropriate process, the reduced graphene oxide (RGO) formed is similar to graphene. However, it still contains residual oxygen and other hetero-atoms, and structural defects [26]. The resulting RGO has been used as starting material for the fabrication of various modified electrodes [27–30], which were then used as electrochemical sensors to determine different analytes in various matrices. Thus, sensors based on immobilized RGO at different electrodes have been developed to determine nitromethane in complex real samples [31], sulfide in fruits [32] or gatifloxacin in tablets and human urine samples [30]. Different RGO modified electrodes have also been used to quantify CA. Thus, Filik et al. [33]. have developed a glassy carbon electrode (GCE) modified with a Nafion/RGO composite film to determine CA in white wine samples. Moreover, Vilian et al. [34]. studied the CA electrochemical oxidation at a GCE modified with chemically reduced GO using different electrochemical techniques. This modified electrode was further used to determine CA in wine samples.

In this paper, we study for the first time the CA electrochemical oxidation in 1.0 M $HClO_4$ and phosphate buffer solutions (PBS) of different pH at a GCE modified with electrochemically partially reduced graphene oxide (GCE/ePRGO). Cyclic (CV) and square wave voltammetries were the electrochemical techniques used. A surface quasi-reversible redox couple was found in all reaction media at this modified electrode. The Box-Behnken design (BBD) statistical experiments and the surface methodology (RSM) were used to optimize experimental variables to generate the GCE/ePRGO [35]. Atomic force microscopy (AFM) and electrochemical impedance spectroscopy (EIS) were used to characterize the surface of modified electrodes. EIS was also used to determine a tentative electrochemical area for the GCE/ePRGO.

On the other hand, the main objective of this work is to perform for the first time a complete characterization of the thermodynamic and kinetics of the surface redox couple in 1.0 M $HClO_4$ at glassy carbon electrodes modified with electrochemically partially reduced graphene oxide. Therefore, we used the methods of the "quasi-reversible maximum" and the "splitting of the net SW voltammetric peak" to obtain information about the thermodynamic and kinetics of the superficial redox couple [36–43]. The adsorption isotherm which best describes the specific interaction of CA with the surface of the modified electrode is also discussed. For comparison, CA electrochemical responses were also studied at bare GCE, and GCE modified with a dispersion of GO (GCE/GO).

2. Experimental

2.1. Reagents

CA, $KMnO_4$, H_2SO_4, H_3PO_4, H_2O_2, HCl, trisodium salt of ethylene diamine tetraacetic acid, ferrocene, $K_4[Fe(CN)_6]$ and $K_3[Fe(CN)_6]$ were purchased from Sigma-Aldrich. $HClO_4$, ethanol, methanol, acetic acid, KCl and KNO_3 were Merck p.a. Acetonitrile was Sintorgan, HPLC degree. Ultrapure water ($\rho = 18\ M\Omega\ cm$) was obtained from a Millipore-Milli Q system. Stock solutions of CA (1×10^{-3} M) were prepared in ethanol, protected from light, and kept in the refrigerator. PBS were prepared using 0.1 M Na_2PO_4H (Merck p.a.) and 0.1 M KPO_4H_2 (Merck p.a.). Working solutions were prepared daily by adding different aliquots of the CA stock solution to 1 M $HClO_4$ aqueous solution or the corresponding PBS of different pH. All reagents were used as received. The percentage of ethanol in all solutions was 5%.

2.2. Apparatus

CV and SWV experiments were performed with an AutoLab PGSTAT 101 potentiostat, controlled by the NOVA1.9 electrochemical software. EIS experiments were performed with an AutoLab PGSTAT 30 potentiostat, controlled by the FRA 4.9 software.

The electrodes were inserted into the cell through holes in its Teflon cover. The working electrodes were a bare GCE and both modified GCE/GO and GCE/ePRGO. A platinum wire and Ag/AgCl, 3 M NaCl (BAS, RE-5B) were used as counter and reference electrodes, respectively. In CV, the scan rate (v) was varied from 0.025 to 0.200 V s^{-1}. In SWV, the amplitude (ΔE_{SW}) was varied from 0.025 to 0.100 V, the staircase step (ΔE_s) was 0.005 V, and the frequency (f) was varied from 5 to 90 Hz.

EIS measurements were performed in solutions containing equal concentrations (1×10^{-3} M) of reduced and oxidized forms of the $[Fe(CN)_6]^{4-/3-}$ redox couple, with 0.1 M KCl as the supporting electrolyte. An amplitude sine wave perturbation of 5 mV was applied to electrodes, whereas the dc potential was set at the formal potential of the redox couple, i.e., $E_f^o = 0.250$ V vs. Ag/AgCl. The ac frequency was varied from 0.5 Hz to 10 kHz. Both, the in-phase (Z´) and out-phase (Z´´) impedance components were extracted from experimental data. Nyquist plots were fitted from a non-linear fitting using two equivalent circuits (see below) [44,45], which can be defined into the FRA electrochemical impedance software. The characteristic parameters of both circuits were extracted from these fittings (see below). Most electrochemical measurements were performed at 25 °C, except those where the effect of temperature on voltammetric signals was studied.

Atomic force microscopy (AFM) images were obtained by using Agilent Technologies 5500 AFM (Agilent Technologies, CA, USA) working in acoustic AC mode using Si probes with force constants around of 40 N/m and resonance frequency in the range of 300–350 s kHz (MikroMasch®, HQ:NSC15/AL BS). The experiments were performed in stationary dry-air atmosphere. Images were treated and analyzed using Gwyddion, open source software for the visualization and analysis of scanning probe microscopy data.

2.3. Preparation of graphene oxide dispersions

GO was synthesized from graphite flakes by using an improved method respect to that developed by Marcano et al. [46]. Thus, 9.0 g of $KMnO_4$ was added at a 9:1 mixture of H_2SO_4 / H_3PO_4 concentrated (180:20 cm^3) with stirring. 1.5 g of graphite flakes were then added to form a uniform suspension, which was stirred and heated at 50 °C during 12 h. The mixture was cooled at 5 °C and poured onto ice (200 cm^3) with 30% H_2O_2 (1.5 cm^3). The filtrate was centrifuged at 4000 rpm during 30 min and the precipitated solid was washed several times with a solution of 30% HCl and subsequently with water. The resulting solid was dispersed in water and dialyzed (dialysis membrane of regenerated cellulose with a molecular weight cut-off around 12–14 kD; Spectra/Por®) against water (18 MΩ cm) until the conductance of the dialyzed solution do not change after 6 h.

2.4. Preparation of electrodes

GCE were polished with alumina slurries of 0.30 and 0.05 μm during 1 min each one, and sonicated in water during 30 s. The polished GCE was modified with a GO dispersion (GCE/GO) by dropping an aliquot of 10×10^{-3} cm^3 of the dispersion on the top of the electrode and allows drying during 30 min at 37 °C. The GCE/ePRGO was generated by cycling the GCE/GO in the potential range between −0.200 V and

−1.700 V at 0.052 V s^{-1} in a 0.2 M pH 7.00 PBS (30 cycles). The optimal conditions to generate GCE/ePRGO were chosen as described in Section 2.5.

The GCE electrochemical area was determined by chronoamperometric measurements using 1×10^{-3} M ferrocene (Fc) + 0.5 M KNO_3 through Cottrell plots [44], using a value of 7.6×10^{-6} cm^2 s^{-1} for Fc diffusion coefficient [47]. An average value of A = (0.098 ± 0.004) cm^2 was determined from measurements carried out with three different electrodes.

A tentative value for the GCE/ePRGO electrochemical area was determined from the constant phase element (CPE_1) obtained from the fitting of Nysquist plots using the Scheme 1b (see below), where $CPE_1 = 1.8 \times 10^{-4}$ S s^n and the value of the constant phase element per unit area (1.28×10^{-4} S s^n cm^{-2}) obtained from Table 1 of Ref [45]. Therefore, a tentative area of 1.4 cm^2 was obtained for the GCE/ePRGO.

2.5. Design of experiments

The RSM, which is an efficient statistical technique for optimization of multiple variables with a minimum number of experiments, consists in the use of a set of designed experiments to obtain an optimal response [35]. The BBD statistical experiment and the RSM were used to investigate the effects of four independent variables on the responses and to determine the optimal conditions to generate the GCE/ePRGO.

The optimization process to modify electrochemically the surface of the GCE with GO, involves studying the response of the statistically designed combinations, estimating the coefficients by fitting the experimental data to the response functions, predicting the response of the fitted model and checking the adequacy of the model. Therefore, the independent variables selected were the scan rate (×1), the number of cycles (×2), the volume of the drop of the dispersion of GO (×3) and dilution of the dispersion of OG (×4). The dependent variables (or objective functions) were the peak current (Y1) and the difference between anodic and cathodic peak potentials (Y2) of cyclic voltammograms recorded for the $[Fe(CN)_6]^{4-/3-}$ redox couple at the GCE/ePRGO after the electrochemical reduction of GCE/GO. Thus, through the implementation of the desirability function, the objective was to maximize Y1 and minimize Y2.

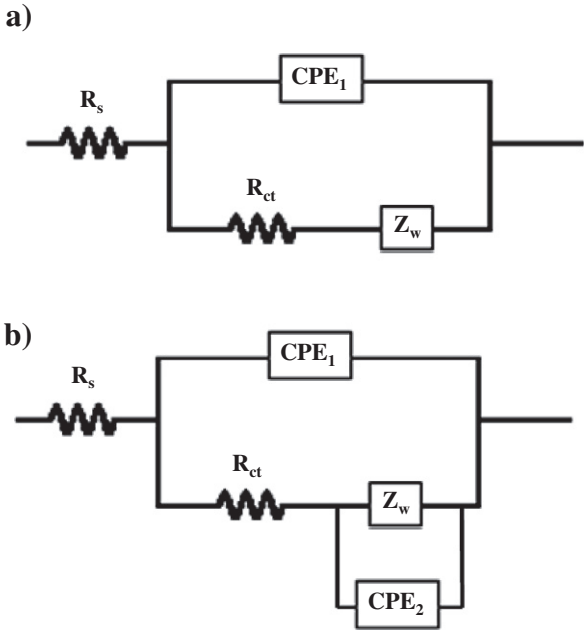

Scheme 1.

Table 1
Independent variable intervals and their levels.

Variables (unit)	Lowest level	Upper level
Scan rate (V s^{-1})	0.01	0.1
number of cycles	1	30
Drop volume dilution of GO (cm^3)	5×10^{-3}	10×10^{-3}
Dilution of the dispersion of GO (GO volume (cm^3): H_2O volume (cm^3))	0.20	0.66

The design model consists of three blocks, with 10 blocks experiments, contemplating six central points. The lowest and upper levels of each variable are shown in Table 1.

From the fit of experimental data, the best model for Y1 was a quadratic model:

$$Y1 = 9.52 \times 10^{-5} - 4.14 \times 10^{-8} X_1 + 2.72 \times 10^{-6} X_2 - 2.13 \times 10^{-6} X_3 - 2.03 \times 10^{-4} X_4 - 1.76 \times 10^{-8} X_1 X_2 - 5.03 \times 10^{-6} X_2 X_4 + 4.12 \times 10^{-8} X_2^2 + 2.78 \times 10^{-4} X_4^2 \quad (1)$$

On the other hand, the best model for Y2 was a model with interactions between two factors, given by:

$$Y2 = 23.76 + 0.62 X_1 + 5.86 X_3 + 237.7 X_4 - 1.41 X_1 X_4 - 21.5 X_3 X_4 \quad (2)$$

Finally, the best conditions for the scan rate, the number of cycles, the volume of the drop of the dispersion of GO and dilution of the dispersion of GO in water were, after the numerical optimization, 0.052 V s^{-1}; 30; 10×10^{-3} cm^3 and 0.66 (GO volume (cm^3): H_2O volume (cm^3)), respectively.

2.6. Characterization of the modified electrodes

The surface morphologies of the GO film before and after of its electrochemical reduction have been characterized by AFM. Fig. 2a and b show a three-dimensional AFM topographies of GO and ePRGO films, respectively. There are slight but distinguishable differences in the topography of both surfaces. The pristine GO film on the carbon electrode (Fig. 2a) presents an uniform wavy surface. This appearance could be a consequence of the stacking and folding of sheets in a disordered manner producing an agglomeration and overlapping, which after drying is observed as a smooth surface waves. The film surface becomes wrinkled, but smoother in the valleys between the wrinkles, after the reduction procedure (Fig. 2b). The surface roughness (Ra) of the GO and ePRGO films for a selected area of 2 × 2 μm were ~15 and ~10 nm, respectively. The electrochemical reductions and other GO reduction methods eliminate oxygenated functional groups, increasing the graphitization with the corresponding increasing in the hydrophobicity and the flake-to-flake π–π interactions [48]. The original waves from GO are observed as sharp winkles in ePRGO, this morphology could be associated to attractive short-range van der Waals and hydrophobic interactions between graphitic domains on the basal planes of the ePRGO sheets. Another difference in the topography of ePRGO is the presence of small and randomly distributed particles, possibly electrolyte crystals trapped into sheets, which cannot be washed after the electro-reduction. The observed differences in surface morphologies between both films have been also reported for GO chemically reduced.

Fig. 3 shows the experimental and fitted Nyquist plots obtained for the bare GCE (Fig. 3a and b), the GCE/GO (Fig. 3c) and the GCE/ePRGO (Fig. 3d). These impedance plots were fitted using the equivalent electrical circuits described in Scheme 1, where R_s is the solution resistance between the working and reference electrodes, R_{ct} is the charge transfer resistance, Z_W is the Warburg element, which represents the linear diffusion of the redox couple to the electrode surface. CPE_1 and CPE_2 correspond to constant phase elements for electrode surfaces without

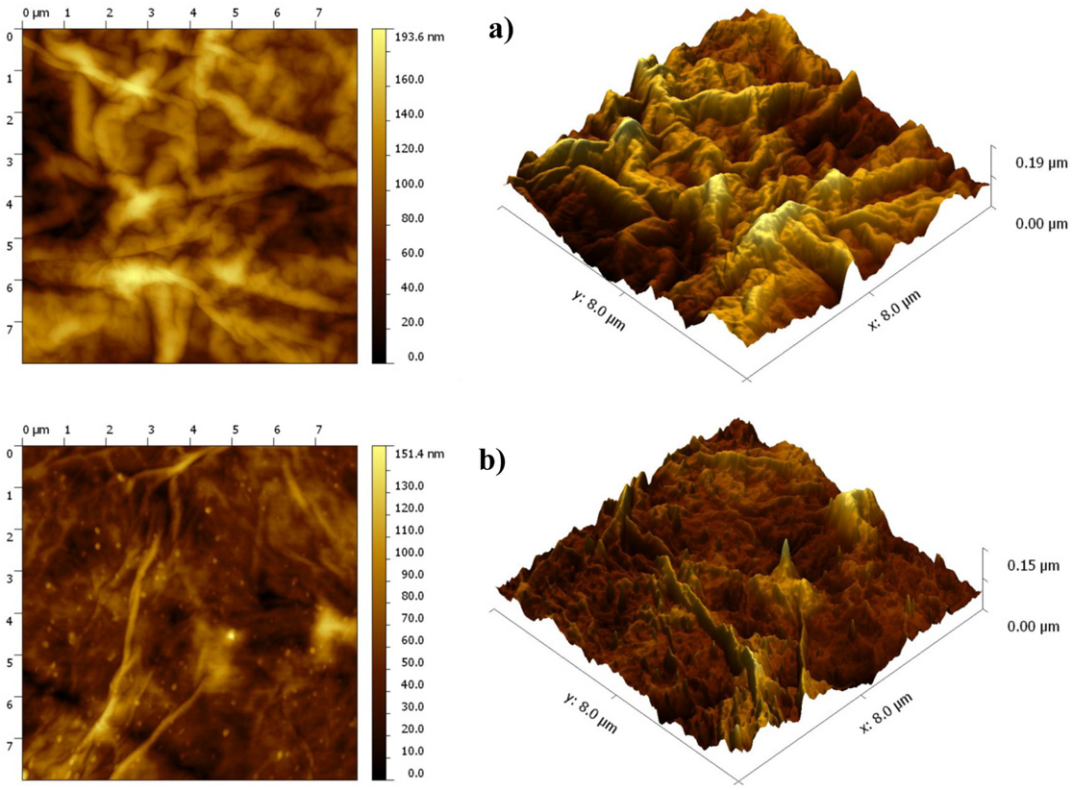

Fig. 2. AFM images obtained for the GCE/GO (a) and GCE/ePRGO (b).

oxygen-containing functional groups and those with oxidized groups, respectively [45]. The best fits of experimental results were obtained with the classical Randles' circuit [44] and the equivalent circuit described in Scheme 1b for the bare GCE and the modified electrodes, respectively. From these results, values of R_{ct} of 196, 520 and 50 Ω were obtained for the bare GCE, the GCE/GO and GCE/ePRGO, respectively.

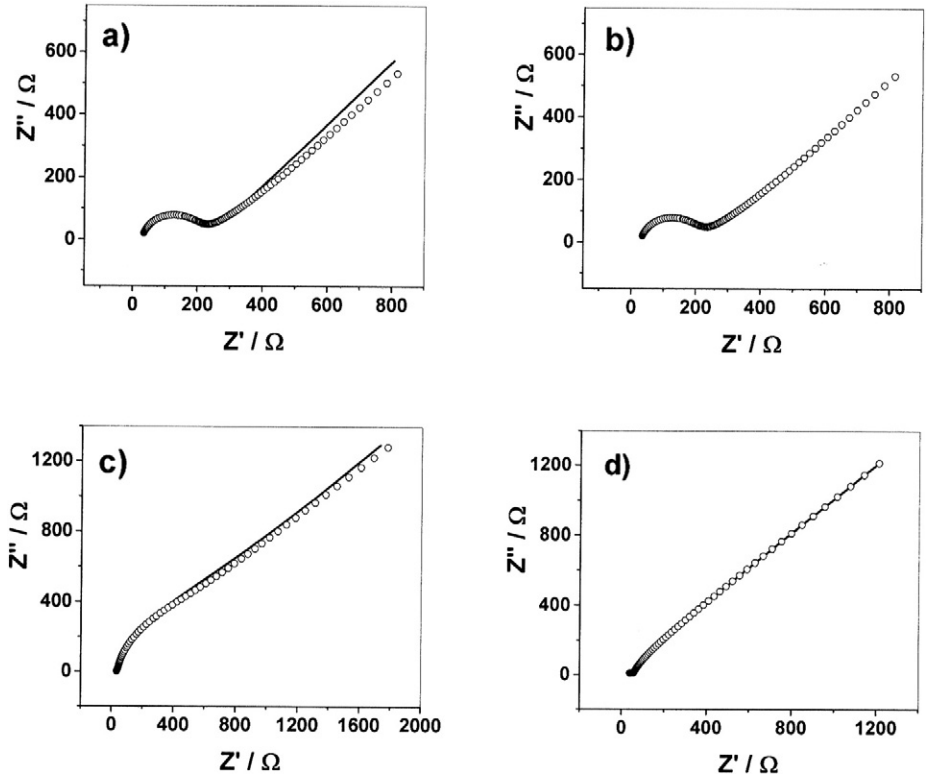

Fig. 3. Experimental (o) and theoretical (solid line) complex plane plots of total impedance of the bare GCE (a and b), the GCE/GO (c) and GCE/ePRGO (d) obtained in the presence of 1.0×10^{-3} M of reduced and oxidized forms of $[Fe(CN)_6]^{4-/3-}$ redox couple + 0.1 M KCl. Reference electrode: Ag/AgCl. $T = 25$ °C. Applied potential: 0.250 V.

The marked decrease in the charge transfer resistance found for GCE/ePRGO might explain the significant improvement obtained in the definition of CA oxidation/reduction peaks at this modified electrode in comparison with those defined at bare GCE and GCE/GO electrodes (see below).

3. Results and discussion

3.1. Cyclic and square wave voltammetries

Fig. 4 shows cyclic voltammograms recorded for CA in 1 M $HClO_4$ at a $c_{CA}^* = 130$ μM at GCE (Fig. 4a), GCE/GO (Fig. 4b) and GCE/ePRGO (Fig. 4c) at a v = 0.050 V s^{-1}. It was applied to each working electrode an accumulation time (t_{acc}) of 600 s at open circuit potential (OCP) in stirred solutions (see below) previously to record the cyclic voltammograms. A

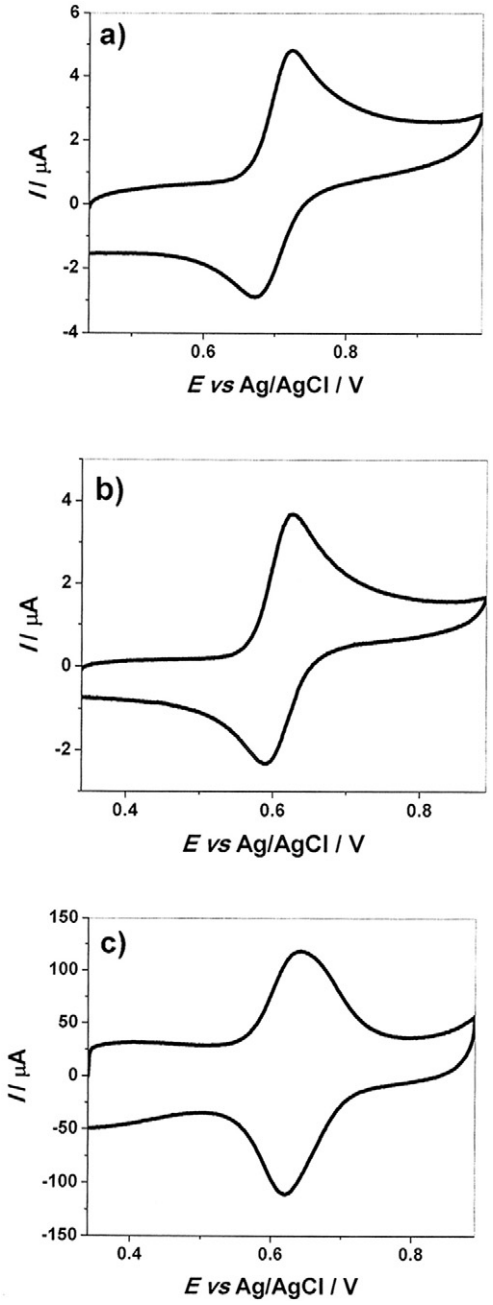

Fig. 4. Cyclic voltammograms ~~of CA~~ recorded in the presence of CA at a) GCE, b) GCE/GO and c) GCE/ePRGO in 1 M $HClO_4$. $c_{CA}^* = 130$ μM. v = 0.050 V s^{-1}. $T = 25$ °C. E_{acc} = OCP = 0.43 V. $t_{acc} = 600$ s.

quasi-reversible redox couple was found for both the bare and modified electrodes. The anodic ($E_{p,a}$) and cathodic ($E_{p,c}$) peak potentials were 0.725 and 0.627 V, respectively, for the bare CGE, with an anodic peak current ($I_{p,a}$) of 4.84 μA (Fig. 4a). A decrease of about a factor of 0.8 in $I_{p,a}$ was found for the CGE/GO respect to the bare GCE, with $E_{p,a}$ = 0.627 V and $E_{p,c} = 0.590$ V (Fig. 4b). Finally, the CA quasi-reversible redox couple showed a significant increase in the current response, being $I_{p,a}$ about 18 times higher than that obtained for the bare CGE, and a slight decrease in the potential compared to the bare GCE and similar to that at the GCE/GO, $E_{p,a} = 0.643$ V and $E_{p,c} = 0.620$ V (Fig. 4c). These results put clearly in evidence a change in the reaction mechanism, showing that the process is mainly adsorption controlled at the GCE/ePRGO [44], which leads to higher sensitivity than those obtained at the bare GCE and GCE/GO. This is probably due to that the electron transfer between the electrode surface and electroactive species in solution is facilitated by the high density of edge-plane-like defective sites at the ePRGO sheets. It is known that the electron-transfer kinetics is generally determined by several factors, including tunnelling and electrostatic and electrocatalytic effects [49].

We also analyzed the effect of the reaction media on the CA electrochemical oxidation at GCE/ePRGO. We found that the intensity of the current increased in all reaction media when cyclic voltammograms were recorded in stirred solutions at different accumulation times (t_{acc}) and at a given accumulation potential (E_{acc}), which was the OCP (see below). Constant current-potential responses were obtained at $t_{acc} = 600$ s for a $c_{CA}^* = 100$ μM. In addition, after recording cyclic voltammograms in solutions in the presence of CA, the working electrode was copiously rinsed with the corresponding blank solution and transferred to another electrochemical cell, which contained only the supporting electrolyte, where quasi-reversible cyclic voltammograms were clearly defined, with current values close to those previously obtained in the presence of CA. These results put in evidence that the overall electrode process is mainly adsorption controlled [44]. In addition, this behavior is expected considering that the cathecol group presents in CA chemical structure (Fig. 1) would be responsible of its electrochemical oxidation, given the corresponding o-quinone as the main product involving 2 e^-, 2H^+, as it was previously discussed [13]. Fig. 5a shows cyclic voltammograms of CA at GCE/ePRGO in 1 M $HClO_4$ and PBS of different pH recorded in the corresponding blank solutions at a given v.

Under these experimental conditions, plots of $I_{p,a}$ vs v were linear for c_{CA}^* in the range from 1.00 to 350 μM, with r values in the range from 0.9876 to 0.9986 for 1 M $HClO_4$ and the different buffers, as it is expected for an adsorption controlled process (results no shown) [44].

In addition, the relationship between charges of the anodic and the cathodic peaks (Qa/Qc) experimentally determined were 1.3, 1.3, 1.2, 1.3 and 1.2 for 1 M $HClO_4$ and PBS of pH 3, 5, 7 and 9, respectively. These results suggest that the cathodic charges are slightly lower than the anodic ones, although relations are close to 1 in all reaction media. This behavior could be explained considering that the electrochemically generated o-quinone would be adsorbed less strongly than the corresponding parent compound and/or the o-quinone would disappear through a chemical reaction coupled to the initial electron transfer reaction. On the other hand, the relationship between charges of the anodic and the cathodic of CA cyclic voltammograms recorded in 1 M $HClO_4$ in the v range from 0.025 to 0.200 V s^{-1} does not show significant changes with the scan rate at a $c_{CA}^* = 130$ μM, with an average value of Qa/Qc = 1.09 ± 0.06.

A decrease in the $I_{p,a}$ was also observed as the pH of the medium increased (Fig. 5a). This behavior could be explained considering that the CA is a triprotic acid (AH_3), so species present in solution will depend on the pH. Thus, the AH_3 species is the only present in solution in the pH range from 0 to 2. Mixtures of AH_3 and AH_2^- and AH_2^- and AH^{-2} species are present in solution in the pH range from 2 to 7 and from 7 to 11, respectively [13]. Based on these results, a likely explanation for the decrease in currents with increasing the pH might be that the CA

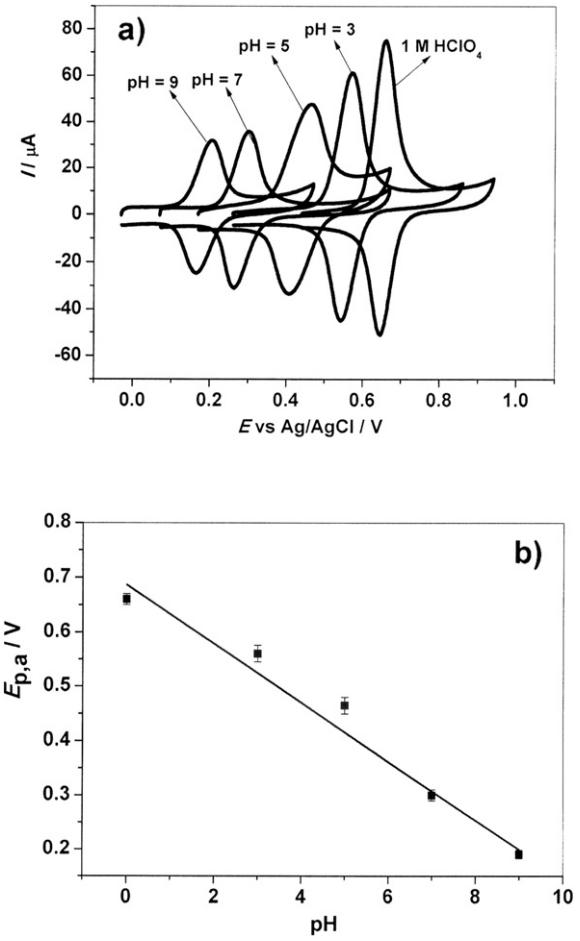

Fig. 5. a) Cyclic voltammograms ~~of CA~~ recorded at GCE/ePRGO in 1 M $HClO_4$ and PBS of different pH after performing the accumulation of CA at the electrode surface in stirred solutions. b) Dependence of the anodic peak potential with the pH. Slope = (0.054 ± 0.005) V/decade, $r = 0.9951$. The c^*_{CA} in the accumulation solution was 100 μM. v = 0.050 V s^{-1}. $T = 25$ °C. E_{acc} = OCP = 0.43 V. t_{acc} = 600 s.

negatively charged species would adsorb less strongly on the modified electrode surface as a result of repulsive forces with the surface of electrode, which will also have a negative charge density with increasing pH due to deprotonation of the oxygenated groups still present in the GCE/ePRGO [26]. In addition, considering that protons are also involved in the electrode process and their availability decreases as the pH increases, the overall reaction rate could be affected.

Values of the difference between the anodic and cathodic peak potentials ($\Delta E_p = E_{p,a} - E_{p,c}$) for the different media were of 0.014, 0.029, 0.056, 0.038 and 0.039 V for 1 M $HClO_4$, and PBS of pH 3, 5, 7 and 9, respectively. From these results, we can infer that the CA surface redox couple has a higher reversibility in the strongly acidic medium.

A shift of the voltammetric peak to less positive potentials was observed as the pH of the medium increased. A variation of the $E_{p,a}$ with the pH of $\partial E_{p,a}/\partial pH = -(0.054 \pm 0.005)$ V/decade (linear correlation coefficient, $r = 0.9981$) was found, indicating that the same number of electrons and protons are involved in the electrode process (Fig. 5b).

In addition, the areas under the oxidation peaks, obtained after subtracting the background currents, represent the charge (Q) associated with the oxidation of CA adsorbed at the electrode surface, i.e.; $Q_{CA} = nFA\Gamma_{CA}$, where n is the number of exchanged electrons per mole of oxidized substance, F is the Faraday constant, A is the electrode area and Γ_{CA} is the surface concentration of CA adsorbed [44].

The specific interaction of CA with the surface of GCE/ePRGO could be explained considering that some functional groups containing oxygen such as epoxides, carbonyls, phenols, carboxyl acids, etc. can still be present at the modified GCE surface [26,50] as it was previously described. The interaction between these functional groups and —OH groups present in the CA chemical structure would be the responsible for the specific adsorption of CA at the GCE/ePRGO.

On the other hand, it is well known that phenols are weak organic acids, and depending on the values of their acid constants, at pH values close to pKa can exist in solution in equilibrium between the parent molecule and some of its phenolate ions. It is well know that oxidation reactions of phenolate ions can be complicated by the presence of dimerization reactions coupled to the initial charge transfer reaction [51,52]. In acidic conditions, the dimerization reactions are largely suppressed and the o-quinone species is the main oxidation product.

Based on these results, the thermodynamic and kinetic studies of the CA redox couple adsorbed at CGE/ePRGO were carried out in 1 M $HClO_4$.

Therefore, studies were conducted to find the most favorable accumulation time (t_{acc}), and the optimum accumulation potential (E_{acc}) for performing the CA pre-concentration step at the electrode surface. Therefore, we recorded cyclic voltammograms of CA in 1 M $HClO_4$ at v = 0.050 V s^{-1} and a $c^*_{CA} = 350$ μM, where the E_{acc} was varied from 0.40 to 0.60 V at intervals of 0.050 V, including the OCP, $E_{OCP} \cong 0.43$ V. No significant change was observed in current and peak potential values as the E_{acc} was varied (results no shown). Thus, the accumulation was conveniently performed at OCP. Therefore, the experiments described below were carried out using an $E_{acc} = E_{OCP} = 0.43$ V. Voltammetric responses showed a good reproducibility and repeatability. Thus, a percent relative standard deviation (RSD %) of (4.0 ± 0.5) % was determined for the $I_{p,a}$ from three cyclic voltammograms obtained at v = 0.050 V s^{-1} with four GCE/ePRGO freshly prepared. Consecutive cyclic voltammograms recorded on the same GCE/ePRGO at a given v showed a very good repeatability of about (2.0 ± 0.3) %. Fig. 6 shows cyclic voltammograms recorded in the presence (a) and in the absence (b) of CA at GCE/ePRGO in 1 M $HClO_4$. The first (line 1) and the second (line 2) scans recorded in the presence of CA are shown in Fig. 6a. The first (line 3) and the tenth (line 4) scans recorded in the corresponding blank solution are shown in Fig. 6b. These results clearly demonstrate the very good reproducibility of the voltammetric signals, and that the current is practically the same in the presence or in the absence of CA.

The effect of the t_{acc} on the $I_{p,a}$ was studied at several c^*_{CA} by using CV. The results obtained at 25 °C for different c^*_{CA} are shown in Fig. 7. $I_{p,a}$ increased up to a plateau level as the t_{acc} was increased for each c^*_{CA} studied.

The saturation $I_{p,a}$ varied depending on the c^*_{CA}.Thus, for the c^*_{CA} lowest concentration studied, stationary currents were achieved at a t_{acc} = 1300 s in 1 M $HClO_4$ at 25 °C (Fig. 7). Therefore, the following experiments were carried out using a $t_{acc} = 1300$ s. In addition, at concentrations higher than 350 μM the electrode was fully covered.

From these results, we calculated values of Γ_{CA} of 1.4×10^{-11}, 2.4×10^{-11}, 1.4×10^{-10}, 2.0×10^{-10}, 5.0×10^{-10}, and 6.1×10^{-10} mol cm^{-2} for c^*_{CA} of 0.1, 1, 5, 20, 100 and 150 μM, respectively, using an average electrochemical area of 1.40 ± 0.03 cm^2. Thus, at lower c^*_{CA}, the adsorbate surface concentration would correspond to a sub-monolayer, while Γ_{CA} values obtained in the concentration range from 5 to 150 μM would correspond to the coverage of a monolayer or even more than a monolayer of adsorbed substrate [44].

In addition, we also studied the dependence of $I_{p,a}$ with t_{acc} at different temperatures (Fig. 8).

Values of higher peak currents were obtained as the temperature was increased, indicating a positive value for the enthalpy of adsorption of CA in 1 M $HClO_4$ at GCE/ePRGO. A similar behavior has previously been found by us for the adsorption of butein on bare GCE's in pH 4.00 citrate buffer solutions [43]. This behavior was also found by Gileadi et al. [53,54]. for the adsorption of ethylene and benzene at gold electrodes. This phenomenon can be explained considering that an increase in entropy can occur during the adsorption of a given substrate from solution, where some solvent molecules should be removed from the electrode surface for each substrate molecule adsorbed [55].

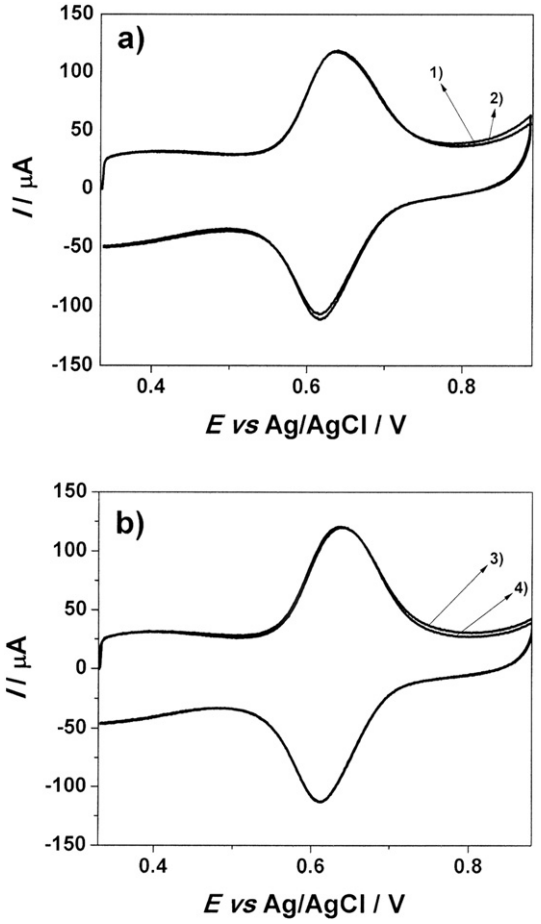

Fig. 6. Cyclic voltammograms recorded in the presence (a) and in the absence (b) of CA at GCE/ePRGO in 1 M $HClO_4$. 1) and 2) are the first and the second scans, respectively. 3) and 4) are the first and the tenth scans, respectively. $c^*_{CA} = 130$ μM. $v = 0.050$ V s^{-1}. $T = 25$ °C. E_{acc} = OCP = 0.43 V. $t_{acc} = 600$ s.

Fig. 9a shows a plot of Q_a vs c^*_{CA}, where Q_a represents the charge associated with the corresponding anodic peak at a given v, after subtraction of any residual current. Practically constant charge values were obtained at a $c^*_{CA} \geq 350$ μM. Moreover, the dependence between c^*_{CA} and the surface coverage (θ) was studied to derive the adsorption isotherm. The surface coverage was defined as $\theta = Q_a/Q_{a,max}$, where Q_a is the charge from cyclic voltammograms obtained for different c^*_{CA} at a $t_{acc} = 1300$ s and $Q_{a,max}$ is the maximum value of Q_a obtained at the

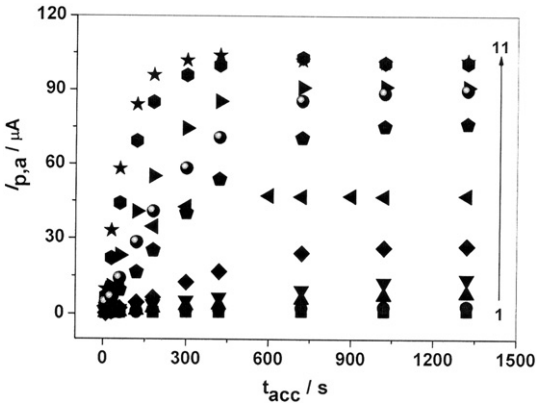

Fig. 7. Dependence of the anodic peak currents with the accumulation time at different CA concentrations. c^*_{CA}(from 1 to 11) = 0.1, 1, 5, 10, 20, 100, 130, 180, 200, 350 and 500 μM. $v = 0.050$ V s^{-1}. $T = 25$ °C. E_{acc} = OCP = 0.43 V.

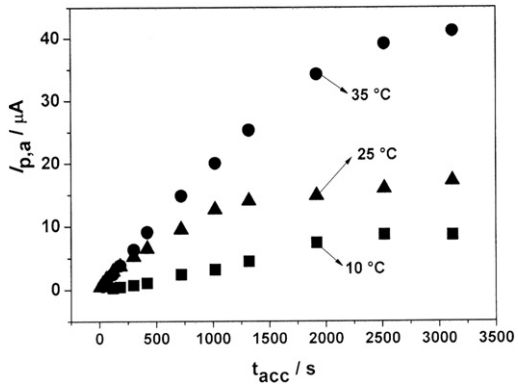

Fig. 8. Dependence of the anodic peak currents with the accumulation time at different temperatures in 1 M $HClO_4$. $c^*_{CA} = 10$ μM. $v = 0.050$ V s^{-1}. E_{acc} = OCP = 0.43 V.

same accumulation time for the highest CA concentration studied, i.e., $c^*_{CA}c^*_{BU} = 350$ μM. A plot of $c^*_{CA}c^*_{BU}$vs θ is shown in Fig. 9b.

Experimental data were fitted to different models of adsorption isotherms (Langmuir, Temkin, Frumkin, Freundlich) with the purpose of finding the best isotherm which describes the specific interaction of

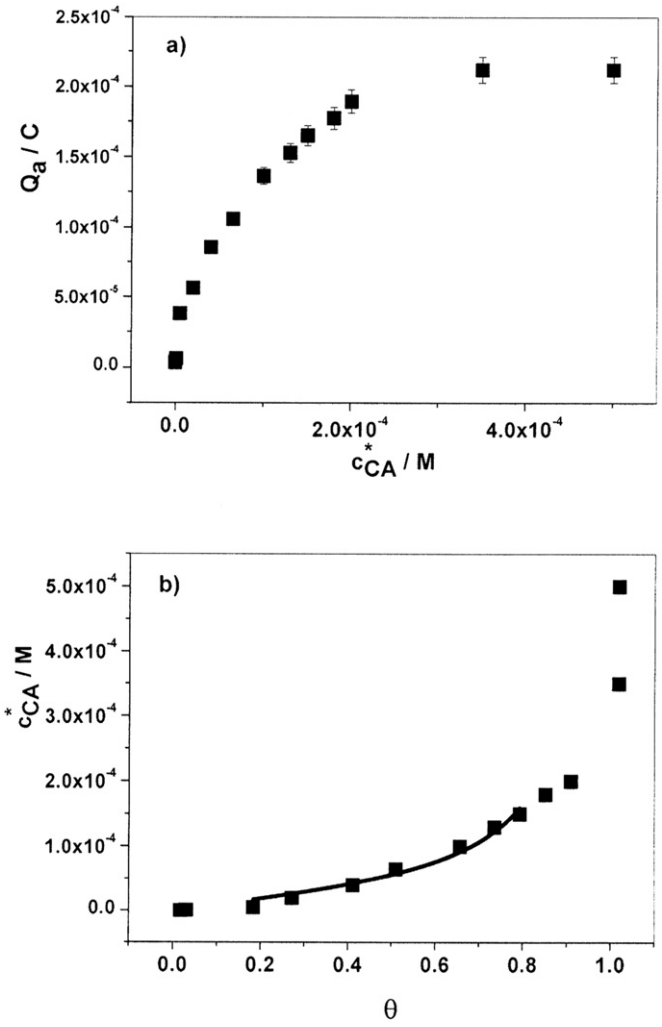

Fig. 9. a) Dependence of the anodic charge with the CA concentration. b) Dependence of CA concentration with the surface coverage, defined as $\theta = Q_a/Q_{a,max}$ (see text). The solid line represents the best fit between experimental and theoretical data obtained when the Frumkin isotherm was chosen to perform the fit. $v = 0.050$ V s^{-1}. $T = 25$ °C. E_{acc} = OCP = 0.43 V. $t_{acc} = 1300$ s.

CA with the surface of GCE/ePRGO. The best fitting was obtained when the Frumkin adsorption isotherm [44,55,56] was chosen to perform the fit. The Frumkin adsorption isotherm gives useful information considering that it takes into account the interactions between adsorbed molecules. It can be expressed as [44,55,56]:

$$\beta c_{CA} = \frac{\theta}{1-\theta} \exp(-g'\theta) \quad (3)$$

Thus, from Eq. (3) it is possible to calculate β and g′, where $g' = 2g\Gamma_{CA,s}/RT$ is the parameter that characterizes the interactions between adsorbed molecules, and g expresses the way in which the adsorption energy changes as a function of the θ. If g is positive, the interactions between adsorbed species are attractive; and if g is negative, the interactions are repulsive. $\Gamma_{CA,s}$ is the CA saturation coverage, and β the adsorption coefficient, which is defined as $\beta = \exp.(-\Delta G_{ads}/RT)$, where ΔG_{ads} is the Gibbs adsorption apparent free energy [44].

The fit was carried out for values of θ in the range from 0.18 to 0.79. The best fit between experimental and theoretical data is shown in Fig. 8b (solid line). From the best fit, values of $\beta = (11 \pm 1) \times 10^3$, $g' = (1.1 \pm 0.3)$ and $\chi^2 = 9.7 \times 10^{-11}$ were obtained. From these results, a value of $\Delta G_{ads} = -22.8$ kJ mol^{-1} was calculated for the Gibbs adsorption apparent free energy. These results indicate that the process of CA adsorption at GCE/ePRGO is energetically favorable and that lateral interactions between the adsorbed molecules are attractive [44]. These results compare reasonably well with those obtained previously in our laboratory for the adsorption of similar compounds [41–43].

A negative value for ΔG_{ads} indicates a higher contribution of the entropy of adsorption than the heat of adsorption. This behavior has also been discussed in literature for other compounds [44,53–55].

On the other hand, from SW voltammograms of a surface redox couple it is possible to determine the thermodynamic and kinetic parameters such as the formal potential (E_f^o), the formal rate constant (k_s) and the anodic electron transfer coefficient ($1 - \alpha$) [36–40].

Therefore, the net currents (I_n) of SW voltammograms of surface redox couples split as the amplitude of the SW increases at a given ΔE_s and f [37,40]. Fig. 10 shows the forward (I_f), reverse (I_r) and I_n currents obtained from SW voltammograms recorded for CA in 1 M $HClO_4$ aqueous solution. A single peak is observed for I_n when $\Delta E_{SW} = 0.025$ V (Fig. 10a). However, as ΔE_{SW} increased the I_n start to split around the E_f^o (Figs. 10b–d). The splitting of the SW net peak allows to calculate E_f^o of the surface redox couple from $E_f^o = ½ (E_{p,f} - E_{p,r})$, where $E_{p,f}$ and $E_{p,r}$ are the peak potentials for the forward (anodic) and reverse (cathodic) scans, respectively. Thus, an average value for the formal potential ($\overline{E_f^o}$) of the CA surface redox couple of (0.638 ± 0.005) V was calculated in 1 M $HClO_4$.

Moreover, the ratio between the forward (anodic) and reverse (cathodic) currents ($I_{p,f} / I_{p,r}$) allows to determine $(1 - \alpha)$ for $(1 - \alpha) > 0.2$ [40]. An average value for the anodic transfer coefficient ($\overline{1-\alpha}$) of (0.58 ± 0.06) was calculated for CA surface redox couple in 1 M $HClO_4$.

On the other hand, if both the reactant and the product of the surface redox couple are strongly adsorbed on the electrode surface, a plot of $I_{p,n}\, f^{-1}$ vs. f shows a maximum (f_{max}), which appears at a frequency approximately equal to k_s of the surface redox couple. In cases where there are lateral interactions between adsorbed molecules, Lovric et al. [40]. defined an apparent formal rate constant ($k_{s,app}$), which depends on the surface coverage θ and the Frumkin interaction parameter (a). Thus, the "a" parameter is equivalent to "g′" parameter in Eq. (3).

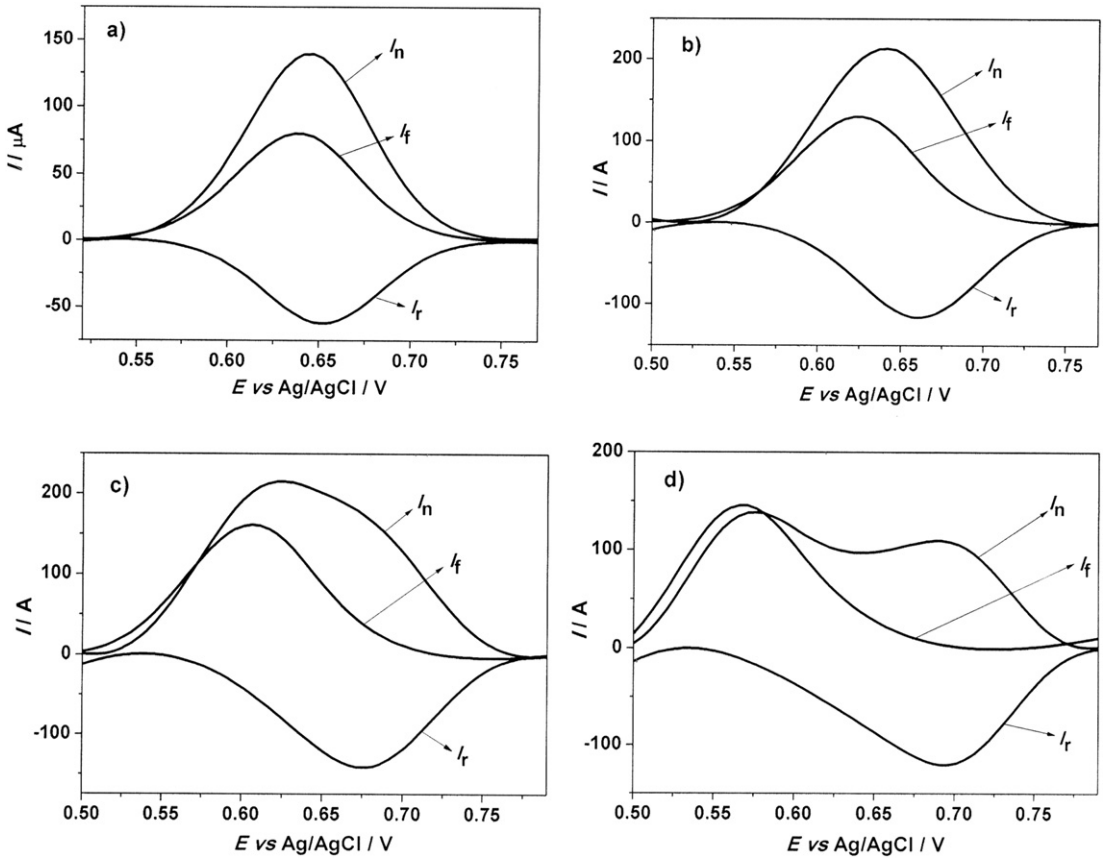

Fig. 10. Net (I_n), forward (I_f) and reverse (I_r) currents of SW voltammograms recorded for CA in 1 M $HClO_4$ at different SW amplitudes. ΔE_{SW} = a) 0.025, b) 0.050, c) 0.075 and d) 0.100 V. $c_{CA}^* = 10$ μM. $T = 25$ °C. $t_{acc} = 1300$ s. $\Delta E_s = 0.005$ V and f = 10 Hz.

Fig. 11 shows plots of $I_{p,n}\ f^{-1}$ vs. f at five θ values. The critical frequency, f_{max}, decreases as the θ increases as it is theoretically expected for a surface redox couple with attractive interactions between the adsorbed molecules [39,40].

The linearized equation which relates f_{max} with k_s, θ and the interaction parameter "a" can be expressed as [40]:

$$\ln(f_{max}) = \ln\frac{k_s}{(\omega_{int})_{max}} - 2a\theta \quad (4)$$

where $(\omega_{int})_{max} = k_{s,app} / f_{max}$, and where $(\omega_{int})_{max}$ values are equals to ω_{max} values for a surface redox couple without lateral interactions between adsorbed molecules. Values of k_s were calculated from Eq. (4) at different θ, using a value of $\omega_{max} = 0.9$, which was extracted from Table 2.3 of reference [40] (for $n\Delta E_{SW} = 0.050$ V and $(1 - \alpha) = 0.6$). A plot of ln f_{max} vs θ (Eq. (4)) was linear in the θ range from 0.17 to 0.53 (four points were taking into account in the regression, $r = 0.9870$), with an intercept of (3.8 ± 0.2) and a slope of $-(3.1 \pm 0.5)$. From the intercept and the slope, values of $k_s = 40\ s^{-1}$ and $a = 1.55$ were calculated, respectively. This value for the interaction parameter is close to that one obtained from the fitting of the best adsorption isotherm ($g' = 1.10$). The error in the estimation of k_s using ω_{max} is close to 10%.

The value of k_s obtained for the CA surface redox couple at GCE/ePRGO in 1 M $HClO_4$ compares reasonably well with the value of k_s obtained for morin adsorbed at GCE in 0.2 M PBS of pH 7 ($k_s = 87\ s^{-1}$) [41] and is approximately one order of magnitude lower than the values determined for rutin adsorbed at GCE in 10% ethanol + 90% 1 M $HClO_4$ ($k_s = 6.1 \times 10^2\ s^{-1}$) [41] and butein adsorbed at GCE in 1 M $HClO_4$ ($k_s = 4.6 \times 10^2\ s^{-1}$) [43].

4. Conclusions

The caffeic acid electrochemical oxidation was studied for the first time in 1 M $HClO_4$ and phosphate buffer solutions of different pH at glassy carbon electrodes modified with electrochemically partially reduced graphene oxide. The Box-Behnken design statistical experiments and the surface methodology were used to optimize experimental variables to generate the modified electrode. Atomic force and electrochemical impedance spectroscopies were used to characterize the surface of modified electrode. Electrochemical impedance spectroscopy was also used to estimate a tentative electrochemical area for the modified glassy carbon electrode.

A surface redox couple was well defined in all reaction media, which showed a very good reproducibility and repeatability. Electrochemical responses were much better defined on this modified electrode compared to those obtained on the bare glassy carbon and the glassy carbon electrode modified with graphene oxide. In addition, surface electrochemical signals were also better defined in the strongly acidic medium (1 M $HClO_4$) than in buffer solutions. These results demonstrate the caffeic acid fully protonated and the corresponding electrochemical generated o-quinone species are more strongly adsorbed at the modified surface electrode than the other species which are present in solution at higher pH, such as anion, dianion, etc.

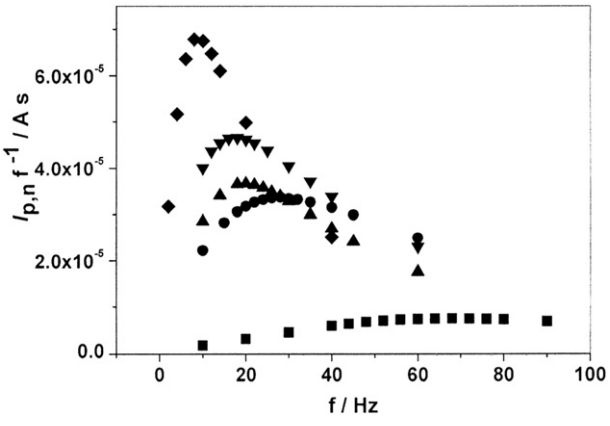

Fig. 11. Plots of $I_{p,n}\ f^{-1}$ as a function of f obtained for CA in 1 M $HClO_4$ at different CA concentrations. c^*_{CA}= (■) 1 (Θ = 0.03, f_{max} = 68 Hz), (●) 5 (Θ = 0.17, f_{max} = 28 Hz), (▲) 10 (Θ = 0.25, f_{max} = 20 Hz), (▼) 20 (Θ = 0.27, f_{max} = 18 Hz) and (♦) 60 μM (Θ = 0.53, f_{max} = 9 Hz). T = 25 °C. t_{acc} = 1300 s. ΔE_{SW} = 0.025 V. ΔE_s = 0.005 V.

Therefore, we performed a complete thermodynamic and kinetics characterization of the surface redox couple in 1 M $HClO_4$. The Frumkin adsorption isotherm was the best to describe the specific interaction between caffeic acid and the modified electrode surface.

In addition, the methods of the "quasi-reversible maximum" and the "splitting of the net square wave voltammetric peak" were used to obtain information about the thermodynamic and kinetics parameters of the surface redox couple.

Acknowledgements

Financial supports from Fondo para la Investigación Científica y Tecnológica (FONCyT, PICT 0916/2010), Consejo Nacional de Investigaciones Científicas y Técnicas (CONICET, PIP 112-201101-00184), Ministerio de Ciencia y Tecnología de Córdoba (MINCYT/Córdoba, PID 2010, Res. 113/2011), and Secretaría de Ciencia y Técnica (SECyT, PPI 2012–2015, Res. 318/12 and 1230/14) from the Universidad Nacional de Río Cuarto are gratefully acknowledged. M. A. Zensich and J. C. López thank to CONICET for doctoral research fellowships. We thank to Reviewers by their valuable suggestions.

References

[1] T. Erk, J. Hauser, G. Williamson, M. Renouf, H. Steiling, F. Dionisi, E. Richling, Biofactors 40 (2014) 103–112.
[2] J.N. Veljkovic, A.N. Pavlovic, S.S. Mitic, S.B. Tosic, G.S. Stojanovic, B.M. Kalicanin, D.M. Stanković, M.B. Stojković, M.N. Mitić, J.M. Brcanović, J. Food Nutr. Res. 52 (2013) 12–24.
[3] W.R. Sousa, C. da Rocha, C.L. Cardoso, D.H.S. Silva, M.V.B. Zanoni, J. Food Compos. Anal. 17 (2004) 619–633.
[4] K. Tyszczuk, A. Skalska-Kaminska, A. Wozniak, Food Chem. 125 (2011) 1498–1503.
[5] M.J. Rebelo, R. Rego, M. Ferreira, M.C. Oliveira, Food Chem. 141 (2013) 566–573.
[6] U.J. Jung, M.-K. Lee, Y.B. Park, S.-M. Jeo, M.-S. Choi, J. Pharmacol. Exp. Ther. 318 (2006) 476–483.
[7] P.-c. Chao, C.-c. Hsu, M.-c. Yin, Nutr. Metab. 6 (2009) 33–40.
[8] N.R. Prasad, A. Karthikeyan, S. Karthikeyan, B.V. Reddy, Mol. Cell. Biochem. 349 (2011) 11–19.
[9] K. Ikeda, K. Tsujimoto, M. Uozaki, M. Nishide, Y. Suzuki, A.H. Koyama, H. Yaasaki, Int. J. Mol. Med. 28 (2011) 595–598.
[10] M.J. Zhang, J. Zhou, L. Wang, B. Li, J.W. Guo, X. Guan, Q.J. Han, H.J. Zhang, Biol. Pharm. Bull. 37 (2014) 347–354.
[11] S. Pradhananga, W.-S. Shim, Eur. J. Pharmacol. 762 (2015) 313–321.
[12] A.M. Granero, H. Fernández, E. Agostini, M.A. Zon, Talante 83 (2010) 249–255.
[13] C. Giacomelli, K. Ckless, D. Galato, F.S. Miranda, A. Spinelli, J. Braz. Chem. Soc. 13 (2002) 332–338.
[14] C. Bianchini, A. Curulli, M. Pasquali, D. Zane, Food Chem. 156 (2014) 81–86.
[15] F.R. Figueirêdo Leite, W.J. Rodrigues Santos, L.T. Kubota, Sens. Actuat. B-Chem. 193 (2014) 238–246.
[16] I.G. David, A.M.C. Bizgan, D.E. Popa, M. Buleandra, Z. Moldovan, I.A. Badea, T.A. Tekiner, H. Basaga, A.A. Ciucu, Food Chem. 173 (2015) 1059–1065.
[17] W. Sordoń, A. Salachna, M. Jakubowska, J. Electroanal. Chem. 764 (2016) 23–30.
[18] K. Tyszczuk, A. Skalska-Kamińska, A. Woźniak, Food Chem. 125 (2011) 1498–1503.
[19] X. Liu, Y. Han, J.W. Evans, A.K. Engstfeld, R.J. Behm, M.C. Tringides, M. Hupalo, H.-Q. Lin, L. Huang, K.-M. Ho, D. Appy, P.A. Thiel, C.-Z. Wang, Prog. Surf. Sci. 90 (2015) 397–443.
[20] M.M. Barsan, K.P. Prathish, X. Sun, C.M.A. Brett, Sens. Actuat. B-Chem 203 (2014) 579–587.
[21] R.S. Sundaram, Graphene (2014) 50–80.
[22] A.T. Najafabadi, Renew. Sust. Energ. Rev. 41 (2015) 1515–1545.
[23] I. Lee, J.B. Joo, M. Shokouhimehr, Chin. J. Catal. 36 (2015) 1799–1810.
[24] Z. Su, H. Wang, K. Tian, F. Xu, W. Huang, X. Tian, Compos. Part A-Appl. S. 84 (2016) 64–75.
[25] M. Hilder, B. Winther-Jensen, D. Li, M. Forsyth, D.R. MacFarlane, Phys. Chem. Chem. Phys. 13 (2011) 9187–9193.
[26] D. Chen, H. Feng, J. Li, Chem. Rev. 112 (2012) 6027–6053.
[27] N. Wang, M. Lin, H. Dai, H. Ma, Biosens. Bioelectron. 79 (2016) 320–326.
[28] W. Qin, D. Li, X. Zhang, D. Yan, B. Hu, L. Pan, Electrochim. Acta 191 (2016) 435–443.
[29] M. Yu, J. Zhang, S. Li, Y. Meng, J. Liu, J. Power, Sources 308 (2016) 44–51.
[30] Z. Jiang, G. Li, M. Zhang, Sens. Actuat. B-Chem 228 (2016) 59–65.

[31] Y. Wen, W. Wen, X. Zhang, S. Wang, Biosens. Bioelectron. 79 (2016) 894–900.
[32] X. Cao, H. Xu, S. Ding, Y. Ye, X. Ge, L. Yu, Food Chem. 194 (2016) 1224–1229.
[33] H. Filik, G. Çetintaş, A.A. Avan, S. Aydar, S.N. Koç, İ. Boz, Talanta 116 (2013) 245–250.
[34] A.T.E. Vilian, S.-M. Chen, Y.-H. Chen, M.A. Ali, F.M.A. Al-Hemaid, J. Colloid Interf. Sci. 423 (2014) 33–40.
[35] N. Kumar, A. Bansal, G.S. Sarma, R.K. Rawal, Talanta 123 (2014) 186–199.
[36] S. Komorsky-Lovric, M. Lovric, F. Z., Anal. Chem. 335 (1989) 289–294.
[37] J.J. O'Dea, J.G. Osteryoung, Anal. Chem. 65 (1993) 3090–3097.
[38] V. Mirceski, M. Lovric, Electroanalysis 11 (1999) 984–989.
[39] V. Mirceski, M. Lovric, R. Gulaboski, J. Electroanal. Chem. 515 (2001) 91–100.
[40] V. Mirceski, S. Komorsky-Lovric, M. Lovric, Square Wave Voltammetry, Theory and Application, Springer, Leipzig, Germany, 2007.
[41] A.Y. Tesio, A.M. Granero, H. Fernández, M.A. Zon, Electrochim. Acta 56 (2011) 2321–2327.
[42] F.E.A. Catunda Jr., M.F. Araujo, A.M. Granero, F.J. Arévalo, M.G. Carvalho, M.A. Zon, H. Fernández, Electrochim. Acta 56 (2011) 9707–9713.
[43] A.Y. Tesio, S.R. Robledo, H. Fernández, M.A. Zon, Bioelectrochem. 91 (2013) 62–69.
[44] A.J. Bard, L.R. Faulkner, Electrochemical Methods: Fundamentals and Applications, second ed. Marcel Dekker, New York, 2001.
[45] E. Casero, A.M. Parra-Alfambra, M.D. Petit-Domínguez, F. Pariente, E. Lorenzo, C. Alonso, Electrochem. Commun. 20 (2012) 63–66.
[46] D.C. Marcano, D.V. Kosynkin, J.M. Berlín, A. Sinitskii, Z. Sum, A. Slesarev, L.B. Alemany, W. Lu, J.M. Tour, ACS Nano 4 (2010) 4806–4814.
[47] M.A. Zon, M. Moressi, L.E. Sereno, H. Fernández, Bol. Soc. Chil. Quím. 39 (1994) 139–151.
[48] M. Pumera, Electrochem. Commun. 36 (2013) 14–18.
[49] A.T. EzhilVilian, S.-M. Chen, Y.-H. Chen, M.A. Ali, F.M.A. Al-Hemaid, J. Colloid Interf. Sci. 423 (2014) 33–40.
[50] S.C. Ray, Application and Uses of Graphene Oxide and Reduced Graphene Oxide, Applications of Graphene and Graphene-Oxide Based on Nanomaterials, William Andrew Publishing, Oxford 2015, pp. 39–55 (Ch. 2).
[51] S. Martinez, L. Valek, Z. Petrovic, M. Metikos-Hukovic, J. Piljac, J. Electroanal. Chem. 584 (2005) 92–99.
[52] D. Nematollahi, M. Rafiee, J. Electroanal. Chem. 566 (2004) 31–37.
[53] E. Gileadi, B.T. Rubin, J.O.'.M. Bockris, J. Phys. Chem. 69 (1965) 3335–3345.
[54] W. Heiland, E. Gileadi, J.O.'.M. Bockris, J. Phys. Chem. 70 (1966) 1207–1216.
[55] E. Gileadi, in: E. Gileadi (Ed.), Electrosorption, Adsorption in Electrochemistry, Plenum Press, New York 1967, p. 15.
[56] J. Lyklema, Fundamentals of Interface and Colloid Science, first ed. Academic Press, London, 1995.